Chimica Techno Acta
published by Ural Federal University
eISSN 2411-1414
chimicatechnoacta.ru

ARTICLE
2026, vol. 13(1), No. 9286
DOI: 10.15826/chimtech.9286

# Microwave combustion synthesis of Co-Ni aluminate spinel for electrophoretic deposition

Khuong T. Truong *, Thach H. Pham, Kien T. Pham, Huy P. Phu

Institute for Tropical Technology (VITTEP), Academy of Military Science and Technology, Ho Chi Minh City 700000, Vietnam

* Corresponding author: ttungkhuong@gmail.com

## Abstract

**Aluminate spinels represent a versatile class of functional materials with potential in catalytic, electronic, and protective coating applications, yet the research on room-temperature, rapid and tunable techniques to form such ceramic coatings remains limited. In this study, $Co_{0.4}Ni_{0.6}Al_2O_4$ powders were synthesized using a microwave-assisted combustion method, so as to examine the influence of different fuel-to-oxidizer (F/O) ratios on combustion behavior, phase formation, and product yield. The results demonstrate that an excess of the fuel leads to localized overheating, carbonaceous residues, and secondary phases, whereas an insufficient amount of fuel results in weak combustion and incomplete crystallization. Among the tested formulations, an F/O ratio of 0.5 produced a highly crystalline spinel phase with no detectable impurities and provided the highest yield, confirming its suitability for efficient spinel formation. The optimized powder was subsequently evaluated for its applicability in electrophoretic deposition (EPD) using an ethanol suspension. Spinel coatings were successfully deposited on SUS 304 stainless steel substrates after different intervals of time. After calcination, ceramic layers were obtained, demonstrating the feasibility of integrating microwave-combusted Co–Ni aluminate spinels into the EPD process. The data revealed that the deposition yield increased steadily with time, while the deposition rate declined, consistent with the characteristic EPD kinetics. This work provides a deeper understanding of the synthesis–deposition pathway and offers foundational insights for the future optimization of Co–Ni aluminate-based ceramic coatings.**

## Key findings

- Optimal F/O ratio of 0.5 allows obtaining pure, highly crystalline $Co_{0.4}Ni_{0.6}Al_2O_4$ with the highest product yield.
- Structural analyses confirm spinel phase formation under optimized microwave combustion conditions.
- EPD successfully produces Co–Ni aluminate coatings with the yield increasing and the deposition rate decreasing over time.



## Accompanying information

**Article history**
**Received**: 24.11.25
**Revised:** 16.12.25
**Accepted:** 21.12.25
**Available online:** 25.12.25

**Keywords**
nitrate salt; glycine; microwave-assisted combustion; alumiate spinel; electrophoretic deposition

**Funding**
This work was supported by Vietnam Academy of Military Science and Technology.

**Supplementary information**
Transparent peer review: READ

**Sustainable Development Goals**
9 INDUSTRY, INNOVATION AND INFRASTRUCTURE

## 1. Introduction

Oxide spinels with the general formula $AM_2O_4$ are an important family of complex binary transition metal oxides that have been widely studied for structural [1, 2], electronic [3, 4], optical [5, 6], catalytic [7, 8], photocatalytic [9–11], and thermal [12–14] characteristics. These variations in properties are largely governed by the types of cations as well as their preferred occupation of specific lattice sites. Within this family, cobalt aluminate ($CoAl_2O_4$) and nickel aluminate ($NiAl_2O_4$) are two technologically significant compounds that offer distinct advantages and functional properties.

Nickel aluminate is a partially antispinel oxide [15] known for its remarkable electronic and thermal stability, making it highly attractive for catalytic and photocatalytic applications. Its energy level structure supports efficient charge transfer and separation, which underpins its strong performance in oxidation reactions, pollutant degradation, and other catalytic transformations [16, 17]. Structurally, $NiAl_2O_4$ typically adopts a spinel-type arrangement where $Ni^{2+}$ cations preferentially occupy tetrahedral sites while $Al^{3+}$ ions sit in the octahedral positions, contributing to its robustness and high thermal resistance. Its high melting point, resistance to deactivation (for example, by coke formation), and stability under harsh reaction conditions make it a promising material for hydrogenation, steam reforming, and other industrial catalytic processes [18, 19]. Cobalt aluminate, in contrast, is perhaps best known for its deeply saturated blue color, which arises from $Co^{2+}$ ions in tetrahedral coordination and the characteristic d–d transitions in its spinel lattice [20]. This colored spinel is not only visually striking but also thermally and chemically stable, which makes it an ideal pigment in ceramics, glazes, glass, and other materials exposed to severe environments [21, 22]. Moreover, $CoAl_2O_4$ can be utilized in other technological applications, such as catalyzing a range of chemical processes [23–25], and sensing water vapor [26], inorganic gases [27], and alcohol compounds [28]. Mixed Co–Ni aluminate spinels can enable synergistic tuning of cation distribution, redox behavior and lattice parameters. They can combine the vivid coloration and stability of cobalt aluminate, together with the electronic conductivity and catalytic robustness of nickel aluminate. Compared to the single-metal counterparts, the composition $Co_{1-x}Ni_xAl_2O_4$ often exhibits enhanced thermal resistance, adjustable electronic conductivity, and strong structural integrity, all of which are desirable traits for ceramic coating applications.

As for preparing spinel nanomaterials, a variety of strategies have been explored, including sol-gel [29, 30], reverse microemulsion [31], hydrothermal [32, 33], and combustion [34-36] methods. Among these, microwave combustion has emerged as a highly promising technique because it provides a straightforward and rapid means of obtaining relatively well-defined spinel materials. This method is also regarded as a cost-effective and tunable approach [37-39]. Compared to the conventional solution combustion synthesis, this method has a different heating mechanism relying on the rapid oscillation of molecular dipoles in the presence of microwaves, allowing volumetric heating of the material, resulting in a more uniform heat distribution [40].

As for producing ceramic coatings, there is an increasing interest in the electrophoretic deposition (EPD) method. EPD is a versatile, room-temperature process capable of forming uniform ceramic layers on conductive substrates, offering advantages such as adjustable thickness, suitability for complex geometries, and rapid deposition rates [41]. Regarding deposition suspension, the benefits of non-aqueous EPD systems (e.g., ethanol or acetone) are highlighted, whereas a disperser, typically iodine, is essential to enhance particle dispersion and surface charging, which allows charged particles to transfer under an electric field and eventually deposit onto an electrode [42]. In recent years, EPD has been applied to fabricate a range of spinel-based coatings, including Mn-Co spinels [43, 44] and ferrites [45]. These studies collectively underscore the growing momentum behind EPD as a practical and scalable route for processing spinel ceramic coatings. Despite this progress, research focusing specifically on aluminate spinel deposition via EPD remains very limited.

In this context, the present work provides further insight into employing microwave combustion for preparing $Co_{0.4}Ni_{0.6}Al_2O_4$ samples with different fuel-to-oxidizer (F/O) ratios. The results indicate the optimal F/O ratio in this case, which is mainly evaluated based on product purity and yield. The spinel powder is then used in the EPD process to deposit spinel coatings. The novel insights mainly lie in exploring the preliminary feasibility of forming such layers on stainless steel substrates. Our findings are expected to provide foundational knowledge for further optimization, performance evaluation, and application-driven development of Co–Ni aluminate spinel coatings.

## 2. Materials and Methods

### 2.1. Materials

All chemicals used in this study were of analytical grade, sourced from Xilong, China, and employed directly without any additional purification. The hydrated nitrate salts included $Co(NO_3)_2{\cdot}6H_2O$, $Ni(NO_3)_2{\cdot}6H_2O$ and $Al(NO_3)_3{\cdot}9H_2O$, while glycine served as the fuel in the combustion process. Iodine acted as a disperser for preparing the spinel suspension.

Commercial SUS 304 stainless steel was used as the material for the electrodes for deposition. Prior to coating, SUS 304 sheets, with dimensions of 20×20×2 mm, were degreased and polished using P120 sandpaper to remove surface oxides. Then, they were subjected to ultrasonic cleaning in acetone (150 W) for 5 min. Subsequently, the plates were dried using either a handheld dryer or an oven.

### 2.2. Synthesis of $Co_{0.4}Ni_{0.6}Al_2O_4$ spinel

A mixture of nitrate salts, $Co(NO_3)_2{\cdot}6H_2O$ (0.8 mmol; 233 mg), $Ni(NO_3)_2{\cdot}6H_2O$ (1.2 mmol; 349 mg), and $Al(NO_3)_3{\cdot}6H_2O$ (4.0 mmol; 1501 mg), was first homogenized in 20 mL of double-distilled water, after which glycine was added, and the solution was stirred continuously for 60 min at 70 °C. The resulting homogeneous solution was then transferred to a porcelain crucible and subjected to microwave irradiation in a domestic microwave oven at 2.45 GHz and 990 W for 5 min. During this process, the solution heated up, water evaporated, and self-ignition occurred,

 DOI: 10.15826/chimtech.9286

producing a brief flame and yielding a solid product along with gaseous byproducts. The obtained solid was subsequently washed three times with pure ethanol to remove residual impurities, dried at 80 °C for 2 h, and finally ground into a fine blue powder.

Various ratios of $Al^{3+}$:glycine were taken, namely 20:9, 15:9, 10:9 and 7:9, and such spinel samples were denoted T1, T2, T3 and T4, respectively.

### 2.3. EPD procedure

A suspension of the spinel material was first prepared by dispersing a 10 g/L spinel mixture in absolute ethanol containing iodine ($I_2$; 0.5 g/L) as a dispersing agent; the mixture was magnetically stirred for 15 min and subsequently ultrasonicated for 30 minutes (180 W). An additional 5 min of ultrasonication (180 W) was conducted before electrophoretic deposition. For deposition, a direct current (DC) power supply was used, with two steel sheets serving as electrodes connected to the positive and negative terminals, respectively. These sheets were positioned vertically, parallel to each other, 1 cm apart, and immersed in the suspension.

At room temperature, a voltage of 60 V was applied during different intervals of 30, 60, 90 and 120 s, corresponding to S30, S60, S90 and S120 coated samples. The steel plate connected to the positive terminal remained uncoated and could be reused for multiple consecutive depositions, whereas the plate connected to the negative terminal gradually accumulated a coating layer as positively charged spinel particles migrated under the electric field. After the deposition, the electrode was carefully and slowly withdrawn from the suspension and dried at 80 °C for 2 h. Subsequently, coated sheets were calcined in an ambient-atmosphere furnace at 800 °C for 2 hours with a heating rate of 4 °C/min.

### 2.4. Characterizations

The crystalline phases of the prepared materials were identified through X-ray diffraction (XRD) analysis (Bruker D2 Phaser) employing Cu Kα radiation (λ = 1.5406 Å). Morphological features were examined using a TESCAN Mira 4 field-emission scanning electron microscope (FESEM, Switzerland) operated at 15 kV. Fourier-transform infrared (FTIR) spectra within the 500–4000 $cm^{-1}$ range were recorded using a Platinum ATR Alpha II spectrometer (Bruker, Germany). Thermogravimetric analysis (TGA) was performed by a TGA-50 analyzer (Shidadzu, USA) under a flow of air.

## 3. Results and Discussion

### 3.1. Synthesis efficiency and structural analysis

Theoretically, metal nitrates react with glycine in the stoichiometric redox reaction to produce spinel, following the equation:

$$0.6Ni(NO_3)_2 + 0.4Co(NO_3)_2 + 2Al(NO_3)_3 + 40/9NH_2CH_2COOH \rightarrow Co_{0.4}Ni_{0.6}Al_2O_4 + 80/9CO_2(g) + 100/9H_2O + 56/9N_2 \quad (1)$$

Equation 1 presents the case of T1 (F/O = 1), whereas F/O ratios of 0.75, 0.5 and 0.35 can be assigned to T2, T3 and T4, respectively. Obviously, the combustion behavior and resulting phase purity of $Co_{0.4}Ni_{0.6}Al_2O_4$ samples were found to depend strongly on the molar ratio of $Al^{3+}$ to glycine used during synthesis. As shown in Figure 1, the four formulations (T1–T4) exhibited distinct visual characteristics, reflecting differences in combustion process and efficiency. As for sample T1, the resulting black-to-dark-blue product displayed surface charring (Figure 1a). The fuel-rich condition produced an overly exothermic reaction, generating local hot spots and promoting partial carbonization of glycine. Such excess fuel is known to lead to incomplete oxidation of organic components during combustion, thereby hindering the formation of a homogeneous spinel phase and yielding a product of poor purity.

A more balanced F/O environment was achieved for T2 and T3, producing a uniformly blue and bright blue powder, respectively, with a porous structure, typical of successful glycine–nitrate combustion (Figures 1b and 1c). In this case, the energy released during combustion was sufficient to sustain self-propagation while avoiding the carbon-rich byproducts observed in T1. In contrast, T4 with the lowest F/O ratio represents an under-fueled composition where insufficient glycine prevented full temperature rise and continuous flame propagation. The combustion reaction proceeded weakly and non-uniformly, resulting in a product dominated by grey, fluffy, unreacted or partially decomposed oxides (Figure 1d), with only a small central region exhibiting the characteristic blue color of the spinel phase (Figure 1e).


**Figure 1** Digital images of (a) T1, (b) T2, (c) T3 and (d, e) T4 spinels after microwave-assisted combustion.

 DOI: 10.15826/chimtech.9286

The very low yield of T4 (roughly 34%) confirms that most of the precursor mixture failed to undergo complete combustion or crystallization. Such insufficient fuel limits the exothermicity of the reaction, leading to incomplete precursor decomposition and poor incorporation of $Co^{2+}$ and $Ni^{2+}$ into the aluminate lattice.

The phase composition of spinel samples further supports the above observations. The XRD patterns of T1, T2 and T3 (Figure 2) exhibit characteristic peaks at 18.88°, 31.16°, 36.76°, 55.59°, 59.36°, 65.22° corresponding to the (111), (220), (311), (400), (422), (511), and (440) planes. These features agree well with JCPDS No. 44-0160 of $CoAl_2O_4$ and confirm the success of the combustion synthesis with the desired mixed-metal aluminate phase. However, the spinel-based peaks of T1 are broad with low intensities, and eventually additional peaks at 42.90°, 62.62° and 51.46° are recorded, corresponding to the (200) and (220) planes of NiO and the (024) plane of α-$Al_2O_3$ (JCPDS No. 00-010-0425) [46]. This once again indicates that excessive glycine promoted local overheating and incomplete cation incorporation into the spinel lattice. These secondary phases are likely a consequence of the inhomogeneous thermal distribution and rapid temperature rise, which can interrupt the solid-state diffusion necessary for homogeneous spinel formation.

On the other hand, spinel-originated patterns of T2 and T3 with sharp and high-intensity peaks confirm the successful formation of a well-crystallized spinel structure (Figure 2). The excellent purity of both samples is verified by the non-existence of impurity phases. Such similarity indicates that decreasing the F/O ratio from 0.75 to 0.5 did not significantly alter the phase composition, but rather influenced the reaction completeness and yield. Particularly, T3 was obtained in a higher yield of 86.09%, compared to that of T2, 74.98%. This implies that the F/O ratio of 0.5 provided the optimal balance between glycine and metal nitrates, promoting complete thermal decomposition, efficient gas release, and uniform temperature distribution throughout the reaction mixture.

The resulting product (T3) exhibited high purity and crystallinity, and also achieved the highest yield.

Regarding the crystallite size of spinel samples, the Scherrer formula (Equation 2) was used, and the calculation was based on the most intensive peak of the spinel phase ((311) plane) [35].

$$D = \frac{0.9\lambda}{\beta \cos\theta}, \quad (2)$$

where $D$ denotes the average crystallite size, λ is the X-ray wavelength, θ represents the Bragg diffraction angle, and β corresponds to the full width at half maximum (FWHM) of the diffraction peak. Accordingly, $D_{311}$ values of T1, T2 and T3 were 10.80, 28.08 and 31.06 nm, respectively. This increasing trend indicates that the decreasing F/O ratio from 1.0 to 0.5 facilitated crystallite growth, resulting in sharper characteristic peaks.

To further confirm that the purified spinel powder contains no combustible components, such as carbon or organic residue, a TGA curve was measured from room temperature to 700 °C with a heating rate of 10 °C/min. As shown in Figure 3, around 5% weight was lost at 700 °C, which can be attributed to moisture evaporation.

## 3.2. Elemental and morphology analysis

Figure 4 presents the FTIR spectra of the synthesized spinel materials. Accordingly, metal–oxygen (M–O) stretching vibrations can be recognized within the 550–700 $cm^{-1}$ region—typical of M–O, Al–O, and M–O–Al bonds (where M denotes Ni or Co) [39]. Specifically, the distinct features at 680 $cm^{-1}$ and 592 $cm^{-1}$ observed in T2 and T3 provide evidence for the successful formation of the cubic spinel aluminate structure. There is an exception of sample T1, which shows a less clearly defined band in this range. FTIR spectrum of T1 also exhibits a weak absorption band near 1601 $cm^{-1}$, corresponding to the bending vibration of H–O–H. Generally, the absence of notable bands associated with organic functional groups further indicates that organic residues were effectively eliminated.

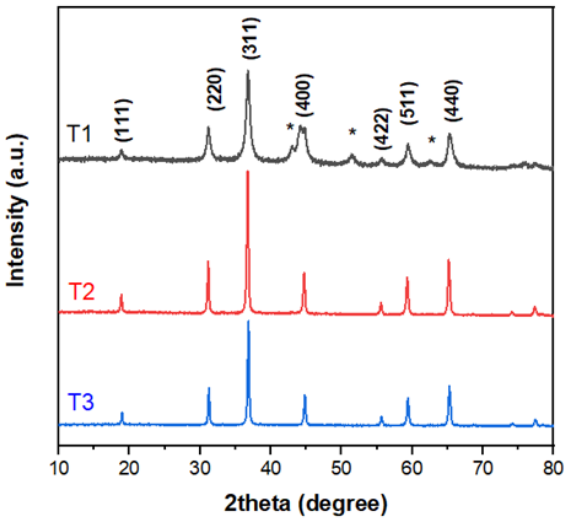


**Figure 2** XRD patterns of T1, T2 and T3 samples.

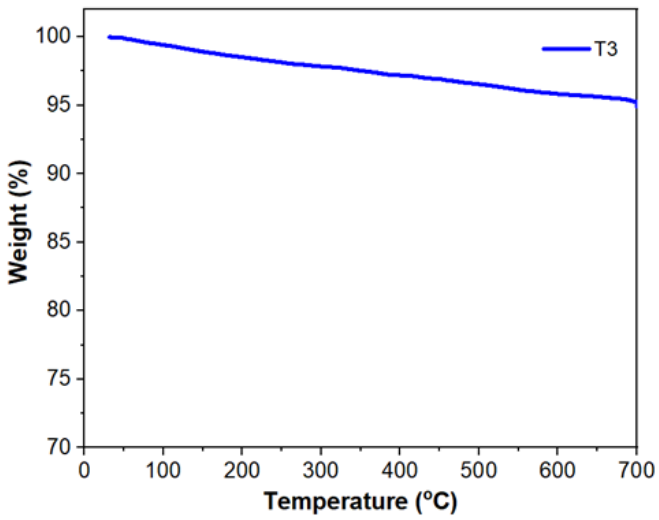


**Figure 3** TGA curve of T3 sample.

 DOI: 10.15826/chimtech.9286

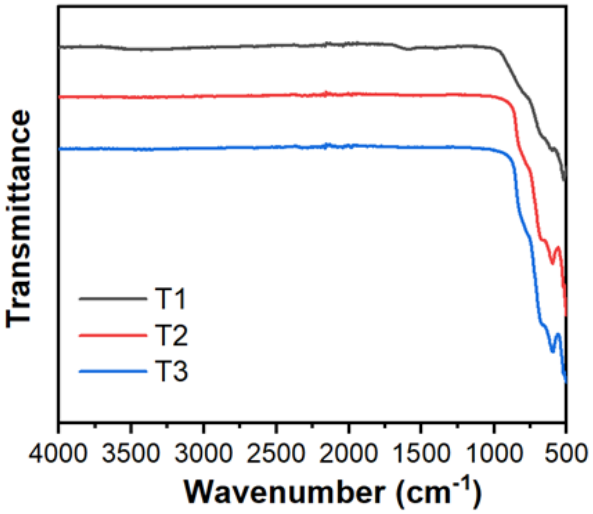


**Figure 4** FTIR spectra of T1, T2 and T3 samples.

**Table 1** Percentages of elements by atomic and weight percentages.

| Element | Atomic % | | Weight % | |
|---|---|---|---|---|
| | T3 | By theory | T3 | By theory |
| Oxygen (O) | 59.03 | 57.14 | 36.67 | 36.21 |
| Aluminum (Al) | 24.44 | 28.57 | 25.61 | 30.54 |
| Nickel (Ni) | 10.29 | 8.57 | 23.44 | 19.92 |
| Cobalt (Co) | 6.24 | 5.71 | 14.28 | 13.34 |

In Figure 5, the EDX spectrum confirms that Al, Co, Ni, and O are the dominant elements presenting in the T3 sample. The corresponding atomic and weight percentages are summarized in Table 1. Interestingly, the material exhibits elemental proportions that closely match the theoretical composition of $Co_{0.4}Ni_{0.6}Al_2O_4$.

FESEM images of T3 (Figure 6) with varied magnifications from 2.00 kx to 50.00 kx reveal that the $Co_{0.4}Ni_{0.6}Al_2O_4$ spinel powders consist of irregular, loosely aggregated particles. The particles exhibit a relatively broad size distribution, generally ranging from submicron fragments to larger agglomerates several micrometers in size. Most particles display rough, porous, and fractured surfaces, typical of materials synthesized via combustion or rapid thermal processes. The morphology can be attributed to incomplete grain growth and rapid gas release during synthesis, leading to the formation of sponge-like clusters and shattered microstructures.

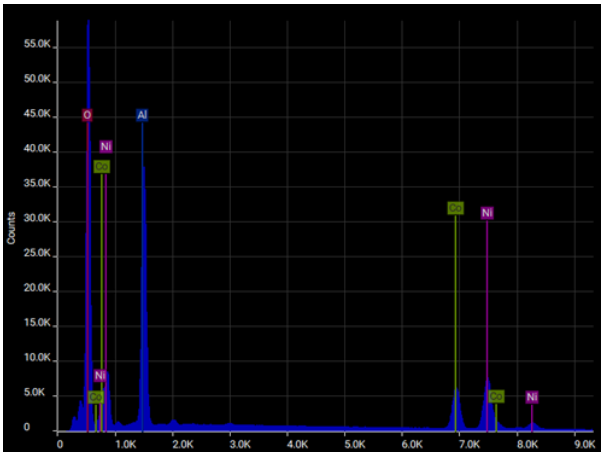


**Figure 5** EDX spectrum of T3 spinel.

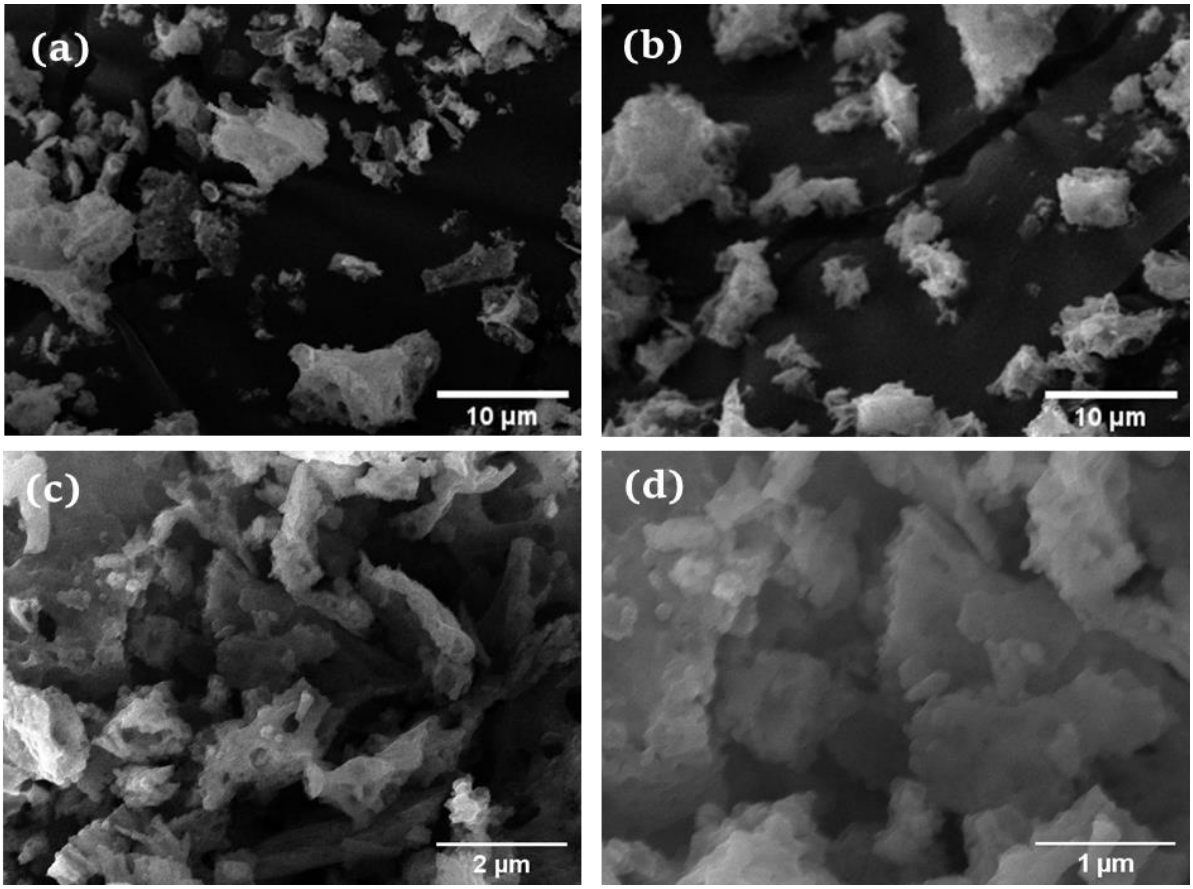


**Figure 6** FESEM images of T3 sample with different magnifications: (a, b) 2.00kx, (c) 20.00 kx and (d) 50.00 kx.

 DOI: 10.15826/chimtech.9286

### 3.3. Deposition efficiency

During the EPD process, an MS1003C DC power supply (Maisheng) was used to maintain a constant voltage of 60 V. T3 spinel was utilized to produce the deposition suspension. The digital image of the EPD system is given in Figure 7a, whereas the coated SUS 304 substrate after drying at 80 °C and calcining at 800°C is shown in Figures 7b and 7c. To further confirm the formation of spinel coating, one side edge of the substrate was polished using P120 sandpaper and imaged with a digital microscope (Figure 7d).

Deposition yield (mg/cm²) was calculated by dividing the weight increase of the substrate by the substrate area (2×2 cm). Similarly, deposition rate (mg·min$^{-1}$·cm$^{-2}$) was obtained by dividing the deposition yield by time. The relationship between deposition time and EPD efficiency is clearly reflected in the trends of both deposition yield and deposition rate (Figure 8). As deposition time increases from 30 to 120 s, the deposition yield steadily rises, indicating continuous accumulation of $Co_{0.4}Ni_{0.6}Al_2O_4$ particles on the electrode surface. This behavior is typical of EPD systems, where longer exposure to the applied field allows more suspended particles to migrate and compact onto the substrate [42, 47, 48].

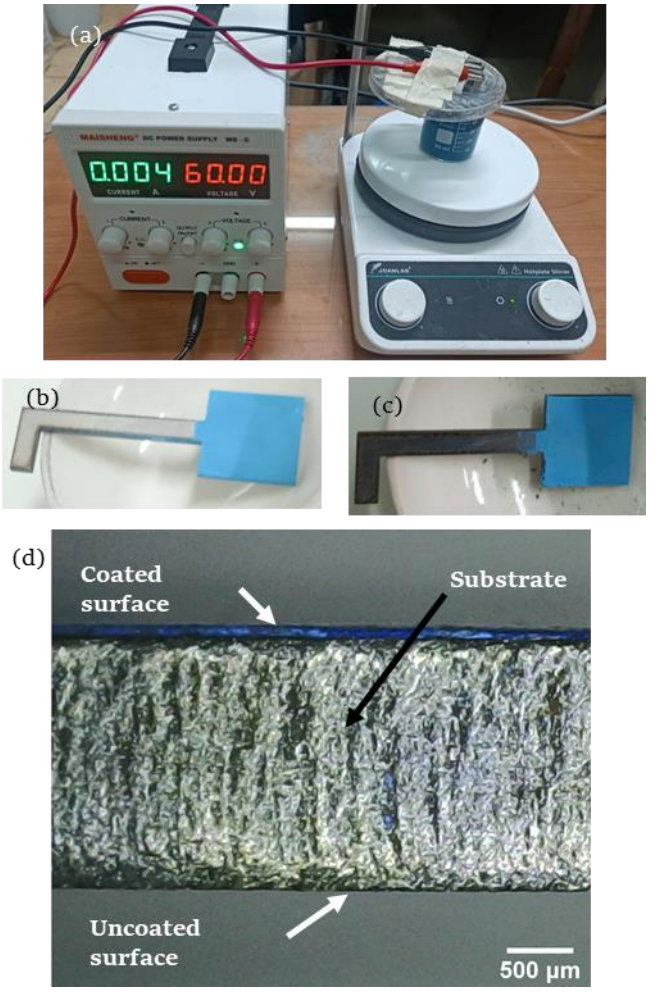


**Figure 7** Practical arrangement of EPD settings (a); Spinel-coated substrate after drying at 80 °C (b) and calcining at 800 °C (c); Capture of one side edge of the coated substrate (d).

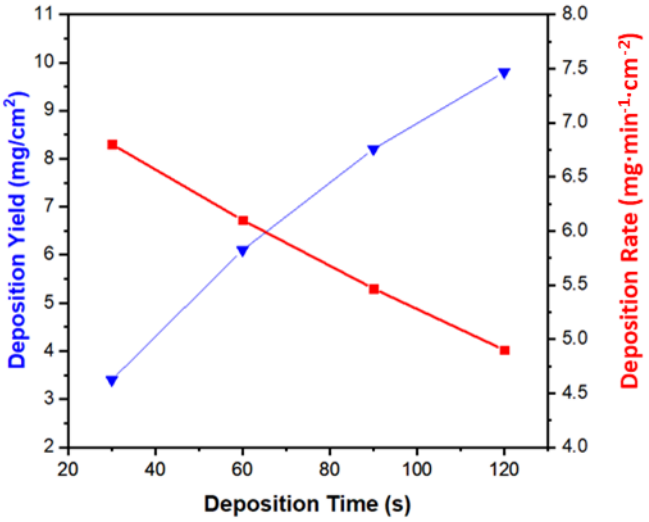


**Figure 8** Demonstration of deposition yield and deposition rate over time.

In contrast, the deposition rate exhibits a progressive decline over the same period, decreasing from its highest value at 30 s to the lowest at 120 s. This tendency also resembles previous literature evidence [42, 47, 48] and suggests that while prolonged deposition enhances overall yield, the process becomes progressively less efficient with time. This reflects a typical kinetic behavior in EPD, where the initial stage is most productive, and efficiency decreases as the deposit thickens. Within the same amount of time, the EPD parameters of this work offer deposition yields that are 3–4 times higher than those achieved in the work with an applied voltage of 30 V and a larger distance between the two electrodes (15 mm) [47]. However, there are studies into Mn–Co and Cu-Mn spinels reporting higher deposition yields, which can be attributed to parameter optimizations, including the utilization of an acetone-ethanol or $H_2O$-ethanol solution and the smaller size of spinel particles [42, 48]. This means that it is possible to further optimize the EPD parameters for Co-Ni aluminate spinels.

## 4. Limitations

As for the microwave synthesis, it is apparent that a large amount of gases ($CO_2$, $N_2$ and $H_2O$) is created for each mole of nitrates. Due to the limited robustness of a domestic oven, a high risk of overpressure presents when more precursors are put in at one time. However, this obstacle to large-scale production can be mitigated with a specialized industrial oven with higher safety standards.

Regarding EPD results, future work should complete certain tasks to further strengthen and expand insights into forming aluminate spinel coatings via the EPD technique. Firstly, other voltages (higher or lower than 60 V) can be tested to compare and confirm the optimal voltage range. Secondly, protective tests in a salty or acidic environment can be performed to precisely evaluate the application potential of the targeted ceramic coating. In addition, future

 DOI: 10.15826/chimtech.9286

systematic experiments related to deposition on large parts with more complex shapes should also be considered to meet the practical requirements.

## 5. Conclusions

This study demonstrated the successful synthesis of $Co_{0.4}Ni_{0.6}Al_2O_4$ spinel powders through a rapid microwave-assisted combustion method, with the F/O ratio playing a decisive role in determining combustion behavior, phase formation, and product yield. An excessive amount of fuel led to localized overheating and impurity formation, whereas an insufficient amount resulted in weak combustion and incomplete crystallization. An F/O ratio of 0.5 was identified as optimal, yielding a highly crystalline, impurity-free spinel with the highest reaction efficiency. Comprehensive structural and compositional analyses confirmed that the optimized product possessed the intended spinel structure, expected elemental ratios, and characteristic porous morphology derived from combustion synthesis.

The suitability of the obtained powder for EPD was further validated. Ethanol-based suspensions enabled the formation of ceramic coatings on SUS 304 substrates, and deposition trends followed typical EPD kinetics, with increasing deposition yield and decreasing rate over time.

Overall, the results confirm that microwave combustion is an effective and rapid route for producing Co–Ni aluminate spinels, and that the resulting materials are compatible with the EPD method for fabricating ceramic coatings. The findings provide a foundational platform for subsequent optimization of coating quality, exploration of different deposition parameters, and future application-driven studies on Co-Ni aluminate protective and functional coatings.

### Supplementary materials

No supplementary materials are available.

### Data availability statement

All related data is included in the manuscript. Nevertheless, raw data related to this study cannot be shared at this time because such data correlates with parts of our ongoing study.

### Acknowledgments

We acknowledge Vietnam Institute for Tropical Technology (VITTEP) for supporting this study.

### Author contributions

Conceptualization: K.T.T., T.H.P.
Data curation: K.T.T., H.P.P., K.T.P.
Formal Analysis: K.T.T., H.P.P.
Funding acquisition: K.T.T.
Investigation: K.T.T., K.T.P.
Methodology: K.T.T., T.H.P.
Project administration: K.T.T.
Resources: K.T.T., T.H.P., H.P.P., K.T.P.
Software: K.T.T.
Supervision: T.H.P.
Validation: K.T.T., H.P.P.
Visualization: K.T.T., K.T.P.
Writing – original draft: K.T.T.
Writing – review & editing: K.T.T, T.H.P.

### Conflict of interest

The authors declare no conflict of interest.

### Additional information

Author IDs:
Khuong T. Truong, Scopus ID 57210428583;
Thach H. Pham, Scopus ID 58805850200.

Website:
Institute for Tropical Technology (VITTEP), Academy of Military Science and Technology, https://vast.gov.vn/web/vietnam-academy-of-science-and-technology/home.

## References

1. Tsurkan V, Krug von Nidda H-A, Deisenhofer J, Lunkenheimer P, Loidl A. On the complexity of spinels: Magnetic, electronic, and polar ground states. Phys Rep. 2021;926:1-86. doi:10.1016/j.physrep.2021.04.002
2. El Jabbar Y, Lakhlifi H, El Ouatib R, Er-Rakho L, Guillemet-Fritsch S, Durand B. Preparation and characterisation of green nano-sized ceramic pigments with the spinel structure $AB_2O_4$ (A = Co, Ni and B = Cr, Al). Solid State Commun. 2021;334-335:114394. doi:10.1016/j.ssc.2021.114394
3. Rafiq M A, Javed A, Rasul M N, Nadeem M, Iqbal F, Hussain A. Structural, electronic, magnetic and optical properties of $AB_2O_4$ (A = Ge, Co and B = Ga, Co) spinel oxides. Mater Chem Phys. 2021;257:123794. doi:10.1016/j.matchemphys.2020.123794
4. Zhandun V S. The magnetic, electronic, optical, and structural properties of the $AB_2O_4$ (A = Mn, Fe, co; B = Al, Ga, In) spinels: Ab initio study. J Magn Magn Mater. 2021;533:168015. doi:10.1016/j.jmmm.2021.168015
5. Ganesh I. A review on magnesium aluminate ($MgAl_2O_4$) spinel: synthesis, processing and applications. Int Mater Rev. 2013;58(2):63-112. doi:10.1179/1743280412Y.0000000001
6. Kushwaha A K, Uğur Ş, Akbudak S, Uğur G. Investigation of structural, elastic, electronic, optical and vibrational properties of silver chromate spinels: Normal ($CrAg_2O_4$) and inverse ($Ag_2CrO_4$). J Alloys Compd. 2017;704:101-108. doi:10.1016/j.jallcom.2017.02.055
7. Zhao S, Guo T, Fan J, Wang L, Han M, Wang J, Wu Y, Chen Y. Versatile Synthesis of Ultrafine Ternary Spinel Oxides/Carbon Nanohybrids toward the Oxygen Reduction Reaction. Energy Fuels. 2020;34(7):9069-9075. doi:10.1021/acs.energyfuels.0c01901
8. Yang S, Gu J, Dai B, Zhang L. A Critical Review of the Synthesis and Applications of Spinel-Derived Catalysts to Bio-Oil Upgrading. ChemSusChem. 2025;18(4):e202401115. doi:10.1002/cssc.202401115
9. Rahmayeni R, Oktavia Y, Stiadi Y, Arief S, Zulhadjri Z. Spinel ferrite of MnFe2O4 synthesized in Piper betle Linn extract media and its application as photocatalysts and antibacterial. J Dispersion Sci Technol. 2021;42(3):465-474. doi:10.1080/01932691.2020.1721011
10. Dom R, Subasri R, Hebalkar N Y, Chary A S, Borse P H. Synthesis of a hydrogen producing nanocrystalline $ZnFe_2O_4$ visible light photocatalyst using a rapid microwave irradiation method. RSC Adv. 2012;2(33):12782-12791. doi:10.1039/C2RA21910G
11. Benlembarek M, Salhi N, Benrabaa R, Djaballah A M, Boulahouache A, Trari M. Synthesis, physical and electrochemical properties of the spinel $CoFe_2O_4$: Application to the photocatalytic hydrogen production. Int J Hydrogen Energy. 2022;47(15):9239-9247. doi:10.1016/j.ijhydene.2021.12.270

12. Ling H, Petric A. Electrical and Thermal Properties of Spinels. ECS Proceedings Volumes. 2005;2005-07(1):1866. doi:10.1149/200507.1866PV
13. Zhao J, Hou Q, Fan B, Zhang L, Zhao F, Luo X, Qi D, Xie Z. Investigation on mechanical and thermal properties of $MgAl_2O_4$-$Mg_2TiO_4$ solid solutions with spinel-type structure. Ceram Int. 2023;49(22, Part A):34490-34499. doi:10.1016/j.ceramint.2023.08.049
14. Braulio M A L, Rigaud M, Buhr A, Parr C, Pandolfelli V C. Spinel-containing alumina-based refractory castables. Ceram Int. 2011;37(6):1705-1724. doi:10.1016/j.ceramint.2011.03.049
15. Sadek H E H, Khattab R M, Gaber A A, Zawrah M F. Nano $Mg_{1-x}Ni_xAl_2O_4$ spinel pigments for advanced applications. Spectrochimica Acta Part A Molecular Biomolecular Spectroscopy. 2014;125:353-358. doi:10.1016/j.saa.2014.01.115
16. Yu X, Wang S, Gao H. Spinel $NiAl_2O_4$ Based Catalysts: Past, Present and Future. J Environ Sci Engin Technol. 2023;11:12-27. doi:10.12974/2311-8741.2023.11.02
17. Salhi N, Boulahouache A, Petit C, Kiennemann A, Rabia C. Steam reforming of methane to syngas over $NiAl_2O_4$ spinel catalysts. Int J Hydrogen Energy. 2011;36(17):11433-11439. doi:10.1016/j.ijhydene.2010.11.071
18. Shokrollahi Yancheshmeh M, Alizadeh Sahraei O, Aissaoui M, Iliuta M C. A novel synthesis of $NiAl_2O_4$ spinel from a Ni-Al mixed-metal alkoxide as a highly efficient catalyst for hydrogen production by glycerol steam reforming. Applied Catalysis B: Environmental. 2020;265:118535. doi:10.1016/j.apcatb.2019.118535
19. Landa L, Remiro A, Valecillos J, Valle B, Bilbao J, Gayubo A G. Performance of $NiAl_2O_4$ spinel derived catalyst + dolomite in the sorption enhanced steam reforming (SESR) of raw bio-oil in cyclic operation. Int J Hydrogen Energy. 2024;58:1526-1540. doi:10.1016/j.ijhydene.2024.01.228
20. Serment B, Brochon C, Hadziioannou G, Buffière S, Demourgues A, Gaudon M. The versatile $Co^{2+}/Co^{3+}$ oxidation states in cobalt alumina spinel: how to design strong blue nanometric pigments for color electrophoretic display. RSC Adv. 2019;9(59):34125-34135. doi:10.1039/C9RA06395A
21. Yaemphutchong S, Wattanathana W, Chansaenpak K, Singkammo S, Kanjanaboos P, Siri-apai P, Janejobsakonkit S, Pipattanaporn P, Suetrong N, Wannapaiboon S, Hanlumyuang Y. Structural investigation and optical properties of cobalt aluminate pigments derived from thermal decomposition of mixed-metal nitrate co-crystals. Ceram Int. 2022;48(13):18490-18501. doi:10.1016/j.ceramint.2022.03.118
22. Gaudon M, Robertson L C, Lataste E, Duttine M, Ménétrier M, Demourgues A. Cobalt and nickel aluminate spinels: Blue and cyan pigments. Ceram Int. 2014;40(4):5201-5207. doi:10.1016/j.ceramint.2013.10.081
23. Zawadzki M, Walerczyk W, López-Suárez F E, Illán-Gómez M J, Bueno-López A. $CoAl_2O_4$ spinel catalyst for soot combustion with $NO_x/O_2$. Catal Commun. 2011;12(13):1238-1241. doi:10.1016/j.catcom.2011.04.021
24. Mo L, Fei J, Huang C, Zheng X. Reforming of methane with oxygen and carbon dioxide to produce syngas over a novel $Pt/CoAl_2O_4/Al_2O_3$ catalyst. J Mol Catal A: Chem. 2003;193(1):177-184. doi:10.1016/S1381-1169(02)00453-3
25. Rojanapipatkul S, Jongsomjit B. Synthesis of cobalt on cobalt-aluminate via solvothermal method and its catalytic properties for carbon monoxide hydrogenation. Catal Commun. 2008;10(2):232-236. doi:10.1016/j.catcom.2008.08.026
26. Vijaya J J, Kennedy L J, Sekaran G, Jeyaraj B, Nagaraja K S. Effect of Sr addition on the humidity sensing properties of $CoAl_2O_4$ composites. Sensors Actuators B Chem. 2007;123(1):211-217. doi:10.1016/j.snb.2006.08.011
27. Michel C R. CO and $CO_2$ gas sensing properties of mesoporous $CoAl_2O_4$. Sensors Actuators B Chem. 2010;147(2):635-641. doi:10.1016/j.snb.2010.04.013
28. Judith Vijaya J, John Kennedy L, Sekaran G, Meenakshisundaram A, Thinesh Kumar R, Amalthi P, Nagaraja K S. Alcohol sensing properties of sol–gel prepared Sr(II)-added cobalt aluminate spinel composites. Sensors Actuators B Chem. 2008;129(2):741-749. doi:10.1016/j.snb.2007.09.031
29. Yu F, Yang J, Ma J, Du J, Zhou Y. Preparation of nanosized $CoAl_2O_4$ powders by sol–gel and sol–gel-hydrothermal methods. J Alloys Compd. 2009;468(1):443-446. doi:10.1016/j.jallcom.2008.01.018
30. Bensemmane N, Medjadji H, Salhi N, Boulahouache A, Derkaoui K, Skender A. Sol–Gel Derived $CoAl_2O_4$ Sheets: Synthesis, Characterization, and Photocatalytic Efficiency for Methylene Blue Degradation under Visible Light. ChemistrySelect. 2025;10(29):e02310. doi:10.1002/slct.202502310
31. Chandradass J, Balasubramanian M, Kim K H. Size effect on the magnetic property of $CoAl_2O_4$ nanopowders prepared by reverse micelle processing. J Alloys Compd. 2010;506(1):395-399. doi:10.1016/j.jallcom.2010.07.014
32. Lu Y, Wang J, He L, Shi Z, Wang X, Zhao K. Hydrothermal synthesis and intrinsic luminescent properties of magnesium aluminate spinel. J Alloys Compd. 2025;1010:178176. doi:10.1016/j.jallcom.2024.178176
33. Aouini S, Bardaoui A, Santos D M F, Chtourou R. Hydrothermal synthesis of $CuMn_2O_4$ spinel-coated stainless steel mesh as a supercapacitor electrode. J Mater Sci Mater Electron. 2022;33(16):12726-12733. doi:10.1007/s10854-022-08219-4
34. Cavalcante P M T, Dondi M, Guarini G, Raimondo M, Baldi G. Colour performance of ceramic nano-pigments. Dyes Pigm. 2009;80(2):226-232. doi:10.1016/j.dyepig.2008.07.004
35. Stella K C, Nesara A S. Low Temperature Soft Chemical Synthesis of Bright Blue CoAl2O4 Spinel Particles. J Nepal Chem Soc. 2010;25(0):62-69. doi:10.3126/jncs.v25i0.3302
36. Azari M, Masoudpanah S M, Alamolhoda S. Solution combustion synthesis of disordered spinel $LiMn_{1.5}Ni_{0.5}O_4$ cathode material using PVP fuel. Electrochem Commun. 2025;177:107945. doi:10.1016/j.elecom.2025.107945
37. Manikandan A, Judith Vijaya J, John Kennedy L, Bououdina M. Microwave combustion synthesis, structural, optical and magnetic properties of $Zn_{1-x}Sr_xFe_2O_4$ nanoparticles. Ceram Int. 2013;39(5):5909-5917. doi:10.1016/j.ceramint.2013.01.012
38. Khattab R M, Sadek H E H, Gaber A A. Microwave Synthesis of $Co_xMg_{1-x}Al_2O_4$ Seed for Pigment Application. Interceram - International Ceramic Review. 2016;65(3):106-110. doi:10.1007/BF03401160
39. Suguna S, Shankar S, Jaganathan S K, Manikandan A. Novel Synthesis of Spinel $MnxCo_{1-x}Al_2O_4$ (x = 0.0 to 1.0) Nanocatalysts: Effect of $Mn^{2+}$ Doping on Structural, Morphological, and Opto-Magnetic Properties. J Supercond Novel Magn. 2017;30(3):691-699. doi:10.1007/s10948-016-3866-7
40. Tompsett G A, Conner W C, Yngvesson K S. Microwave Synthesis of Nanoporous Materials. Chemphyschem. 2006;7(2):296-319. doi:10.1002/cphc.200500449
41. Hu S, Li W, Finklea H, Liu X. A review of electrophoretic deposition of metal oxides and its application in solid oxide fuel cells. Adv Colloid Interface Sci. 2020;276:102102. doi:10.1016/j.cis.2020.102102
42. Ekhlasiosgouei O, Smeacetto F, Molin S. Suspension and process parameters selection for electrophoretic deposition of Mn–Co spinel coating on steel interconnects. Int J Hydrogen Energy. 2024;60:1054-1067. doi:10.1016/j.ijhydene.2024.02.252
43. Sabato A G, Zanchi E, Molin S, Cempura G, Javed H, Herbrig K, Walter C, Boccaccini A R, Smeacetto F. Mn-Co spinel coatings on Crofer 22 APU by electrophoretic deposition: Up scaling, performance in SOFC stack at 850 °C and compositional modifications. J Eur Ceram Soc.

2021;41(8):4496-4504. doi:10.1016/j.jeurceramsoc.2021.03.030
44. Kim S H, Kim D, Oh S-U, Lee J-A, Heo Y-W, Lee J-H. Enhanced performance of Zn-modified $(MnCo)_{1.5}O_4$ spinel coatings: Investigating critical properties for SOFC interconnect materials. Int J Hydrogen Energy. 2025;102:444-451. doi:10.1016/j.ijhydene.2025.01.103
45. Ekhlasiosgouei O, Bik M, Molin S. Preparation of $MnCo_2O_4$ and $Mn_{1.7}CuFe_{0.3}O_4$ single-layer, and novel $MnCo_2O_4$/$Mn_{1.7}CuFe_{0.3}O_4$ dual-layer spinel protective coatings on complex-shaped metallic interconnects by EPD method. Int J Hydrogen Energy. 2024;83:563-576. doi:10.1016/j.ijhydene.2024.07.447
46. Wei Z, Qiao H, Yang H, Zhang C, Yan X. Characterization of NiO nanoparticles by anodic arc plasma method. J Alloys Compd. 2009;479(1):855-858. doi:10.1016/j.jallcom.2009.01.064
47. Chi B, Li J, Yang X, Lin H, Wang N. Electrophoretic deposition of $ZnCo_2O_4$ spinel and its electrocatalytic properties for oxygen evolution reaction. Electrochimica Acta. 2005;50(10):2059-2064. doi:10.1016/j.electacta.2004.09.014
48. Mazur Ł, Domaradzki K, Winiarski P, Zych Ł, Brylewski T. Optimization of electrophoretic deposition and thermal treatment of Cu–Mn spinel matrix for spinel/perovskite composite coating used as SOC metallic interconnect. Ceram Int. 2024;50(18, Part B):34017-34026. doi:10.1016/j.ceramint.2024.06.221

 DOI: 10.15826/chimtech.9286